

# INSTRUMENT DESIGN TEAM PROJECT

---

## SURFACE PROFILOMETER

---

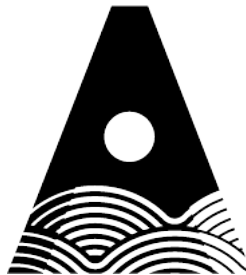
CONDUCTED BY

**MARK ROE**

Student No. G00440145

IN COLLABORATION WITH

**Nicole Murray**  
**Niall Linnane**



### Abstract

This eight-week project encompasses the design and development of an instrument, from conception to its fully functioning form. The device is capable of scanning and generating the topographical height matrix for objects adhering to specified parameters. The specific scope of this report details the cantilever and strain gauge deflection apparatus, utilized for height measurement, and its physical and programmable integration into the greater unit, inclusive of a tri-axial stepper motor system and laser deflection array. The final outcome demonstrates the 3D surface profile produced and the encouraging recreation of the test pieces distinctive contours.

Submission Date: March 12th, 2025

A THESIS SUBMITTED IN PARTIAL FULFILMENT  
OF THE REQUIREMENTS FOR THE DEGREE OF  
**BACHELOR OF SCIENCE IN PHYSICS & INSTRUMENTATION**

---

---

SCHOOL OF SCIENCE & COMPUTING  
DEPARTMENT OF COMPUTER SCIENCE AND APPLIED PHYSICS  
ATLANTIC TECHNOLOGICAL UNIVERSITY, GALWAY

---

---

**SUPERVISORS:**

Dr. Brian Ashall  
Dr. Jennifer Quirke  
Dr. Oran Morris

# Contents

<b>1</b>	<b>INTRODUCTION &amp; THEORY</b>	<b>1</b>
1.1	PROJECT INTRODUCTION . . . . .	1
1.2	APPLICABLE THEORY . . . . .	2
<b>2</b>	<b>METHODOLOGY</b>	<b>6</b>
2.1	APPARATUS . . . . .	6
2.2	CALIBRATION . . . . .	7
2.3	SOFTWARE IMPLEMENTATION . . . . .	8
2.4	TESTING PROCEDURE . . . . .	9
<b>3</b>	<b>RESULTS &amp; ANALYSIS</b>	<b>10</b>
3.1	DEFLECTION MEASUREMENT . . . . .	10
3.2	ERROR ANALYSIS . . . . .	11
3.3	TOPOGRAPHICAL OUTPUT . . . . .	14
<b>4</b>	<b>DISCUSSION &amp; CONCLUSION</b>	<b>16</b>
4.1	SUMMARY OF FINDINGS . . . . .	16
4.2	FUTURE IMPROVEMENTS & APPLICATION . . . . .	16
<b>5</b>	<b>BIBLIOGRAPHY</b>	<b>18</b>
<b>6</b>	<b>PLAGIARISM DECLARATION</b>	<b>19</b>
<b>7</b>	<b>APPENDIX</b>	<b>20</b>

# 1 INTRODUCTION & THEORY

## 1.1 PROJECT INTRODUCTION

The overarching goal of this project is to design and develop a device, capable of producing a 3-Dimensional digital reproduction of a given objects topography. The chosen components to carry out such a procedure, the design process of which will be detailed here, include a cantilever and laser tandem working in conjunction with a tri-axial stepper motor system. The cantilever tip, traversing the test surface through the performance of a raster scanning pattern, will respond to the given contours, inducing a forced deflection on the free end of cantilever. Strain gauge technology mounted on the cantilever represents the primary indicator for this variance.

Motivation for the development of such a device comes in a multitudinous form. The prospect of the highly mechanical nature of the device itself in conjunction with the vitally important software aspect invites oneself to apply a wide-ranging set of skills, crucial for the successful completion of the project. Additionally, while initially presenting itself as a rather straightforward process, the emphasis on harmonious cooperation between each separate component proves a worthwhile and challenging complexity. While the exact real world parallels of this device are few in nature, the comparable principles which apply here have a striking overlap with another device. Within the field of Scanning Probe Microscopy (SPM), the Atomic Force Microscope (AFM) operates in a highly comparable manner [1]. Though in that case, force interactions of the cantilever-tip device on the nano-scale are utilized in lieu of mechanical interaction . To hastily draw comparison, the device being proposed here is to the AFM, as ones finger reading Braille is to a record player's stylus. The same principles with differing resolution ideals.

Though the target of the surface profilometer here is to produce topographical maps on a macro-scale, the dimensions of any given test piece are restricted due to various parameters. The root cause for which each of these restrictions arise will be detailed here. Given the nature of these restricting circumstances, the primary focus of the device turns to the maintenance of accuracy. With that being said, it is worth noting that this project aims to stand as a conceptual proof that such a device is worthwhile, or indeed possible in such a manner. In the wake of analysis, possible improvements will be proposed should this concept be further investigated.

As prefaced on the titlepage, it is pertinent to iterate that this project is a wholly collaborative endeavour. No one member of the team undertaking this project usurps the other, which compounds the importance of cohesion both between team-members as well as the constituent components each oversees in the project. With that, an outline as to which apparatus, and or process, falls under the governance of each member ought to be set forth. The author, Mark Roe, is responsible for the cantilever height detection. Niall Linnane, is responsible for the z-axis motion along with the laser and photodiode array. Finally, Nicole Murray is responsible for the x-y-axis motion and raster scanning procedure. Naturally, this report pertains in large part to the former apparatus, the cantilever height deflection. This component will be of utmost interest here, though of course, will be framed in the broader context of the overall system. For perspective focussing on the two alternate mechanisms, see equivalent reports by Niall Linnane and Nicole Murray.

As a final note with regard to this report, all images of the physical device along with code samples and data tables may be found in the accompanying appendix, Section 7.

## 1.2 APPLICABLE THEORY

The relevant theoretical concepts pertaining to the cantilever device, inclusive of each constituent part, will now be outlined. Possible alternative methods and the rationale for their exclusion from the selection process will be justified. Once each component has been addressed, this process will culminate in the fully realized device design, for the benefit of the reader moving forward.

### STRAIN GAUGES

[2] As indicated in Section 1.1, strain gauges will play the primary role in the detection of strain on the cantilever and thus indirectly the deflection of the adjoining tip.

The essential workings of the common linear strain gauge are quite straightforward. The gauge consists of a strain-sensitive resistive bridge, the elements in which experience a very slight change in resistance in response to an applied mechanical strain. The particular model chosen here, the RS Pro Low Profile Strain Gauge<sup>[3]</sup>, has a resistance value of  $120\Omega$  but an equally frequent value of these devices is the  $350\Omega$  alternative. In this case the former was the choice of preference, due to the higher sensitivity accompanying them as a result of the naturally higher current flow afforded by lower resistance. While the latter offers a lower thermal noise, given the short lifetime of this particular project, this factor should not prove altogether significant. With this in mind it is worth noting that external temperature control plays a lesser though nevertheless significant role in the heating of these devices. Having said that, the recommended temperature range of  $-30^\circ C$  to  $+80^\circ C$  is more than suitable here.

As alluded to earlier, these device only experience a slight change in their resistive response to strain. To elaborate on this, the typical strain gauge, when biased with  $+5V$  differential voltage across the bridge, produces a

voltage merely in the range  $\pm(5 - 10)V$  in response<sup>[4]</sup>. The need for a differential amplifier thus proves entirely appropriate if these voltage output values are to be worked with. Though this is the typical response of the gauges it is not necessarily indicative of what ought to be expected from those utilized here. The Gauge Factor (GF) of the chosen strain gauge is  $2.0$ <sup>[5]</sup>. According to the GF formula in Equation 1, the maximum resistance change for a given mechanical strain can be calculated quite simply<sup>[6]</sup>.

$$GF = \frac{\Delta R/R}{\epsilon} \quad (1)$$

If an approximation is made for a maximum mechanical strain here of  $\epsilon = 1mm/m = 1.0 \times 10^{-3}$ , we can calculate the expected  $\Delta R$ :

$$\begin{aligned} \Delta R &= R \cdot GF \cdot \epsilon \\ \Delta R &= (120)(2.0)(0.001) = 0.24\Omega \end{aligned}$$

The subtle change in resistance highlights once more the accuracy required in measurement, in addition to the necessitation of a robust amplification stage.

While the use of such a strain gauge was included in the original proposition for this project, the plan for their use has been noticeably altered. Originally the idea was touted for four such strain gauges to be mounted onto the cantilever in a quadrant formation. The problems arising out of such a configuration will be addressed in due course, once the Wheatstone Bridge has been introduced. A final consideration here is to establish the optimal location of the strain gauge on the cantilever. As a result of the strain equation, Equation 3 below, a linear relationship emerges, following that increases with proximity to the fixed end.

$$\epsilon(x) = \frac{F(L-x)y}{EI} \quad (2)$$

A useful depiction of the strain along the cantilever can be observed in Figure 2 below. This graphic highlights, what intuition may already suggest, that the greatest strain is experienced at the point at which the cantilever is fixed. In actuality of course, the strain gauge cannot be placed at this point, but rather, it ought to be fixed as closely to it as possible for the greatest reaction to deflection.

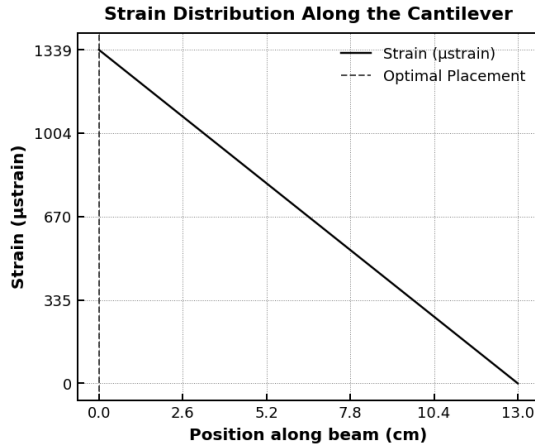


Figure 1: Distribution of strain along the cantilever for a force experienced at the free-extremity

## WHEATSTONE BRIDGE

[7] A Wheatstone Bridge was favoured here from the outset for the application of sensing and exciting the relative ohmic variations. Before delving into the workings of the circuit, a potential alternative that was considered here was that of a direct measurement approach. In such a case, a constant current source would be applied to the bridge and subsequent resistance changes would in turn force a change in potential difference. In these circumstances, a simple non-inverting amplifier would be opted for as a consequence. A great deal of consideration for this method was not necessary. Besides needing to maintain a highly precise current source

for accuracy, this would also close the door to any potential use of a multiple strain gauge configuration. Testing the plausibility of multiple gauges was a much desired goal, to be elaborated on in due course.

The Wheatstone Bridge itself, seen in Figure 1, is presented in this diamond shape of resistor connections with a potential difference held across two of the nodes. It subsequently allows for the determination of an unknown resistor value where the others are held constant, this represents a quarter bridge configuration. It can also be extended in theory to a full bridge configuration, wherein all four legs of the bridge are variable resistance sources. The output of the bridge, measured across the two non-excited nodes, is calculated in accordance with Equation 2<sup>[8]</sup>.

$$V_{out} = V_{exc} \times \left( \frac{R_2}{R_1 + R_2} - \frac{R_4}{R_3 + R_4} \right) \quad (3)$$

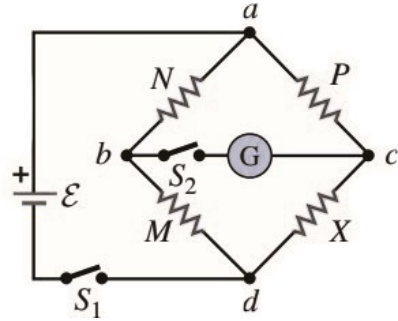


Figure 2: Distribution of strain along the cantilever for a force experienced at the free-extremity

## BRIDGE CONFIGURATION SELECTION

As an extension of what has just been discussed in the previous paragraph, a brief discussion on the selection of the most suitable bridge configuration for this application is necessary. While the quarter bridge configuration, wherein a single strain gauge is accompanied by three comparable non-varying

resistors, naturally presents itself as easier route, the allure of attempting to utilize a full bridge configuration certainly existed. The proposition for using four strain gauges in the bridge is as follows. Given that all four of the resistance values change in response to the mechanical strain applied, the output voltage is maximized. This larger change in turn aids an improved Signal to Noise Ratio (SNR), important for resolution considerations. An additional advantage is the negation of the potential thermal effects, with each identical strain gauge experiencing such effects in equal proportion.

The ultimate downside to this configuration, however, is that in reality many physical effects contribute to the often unstable fluctuations observed. Where gauges are misaligned or bonded to the cantilever in a non-uniform manner, slight variations in resistance characteristics can occur. The uneven distribution of strain across the cantilever will also amount to disproportionate responses across of the bridge, which post-amplification can lead to larger variation. Many of the aforementioned issues are not applicable or else negligible in a quarter bridge configuration. For that reason, the calibration and maintenance of accuracy becomes a far easier and controllable task.

Though an exploration of all possible configurations was conducted, it was decided ultimately, that a middle ground was most appropriate here. Rather than increased risk of fluctuation brought on by the full configuration or conversely the loss of SNR where the quarter bridge is concerned, the half-bridge configuration was settled for. The balanced output observed when employing the two strain gauges, facing opposite one another toward the fixed end, undoubtedly provided the most trustworthy response to stronger deflections.

## SIGNAL AMPLIFICATION

As prefaced in previous sections the necessary next component for the viability of this apparatus is an amplification circuit. To reiterate, the expectation for the output across the Wheatstone Bridge is in the region of  $\pm(5 - 10)mV$ . As such, to create a usable signal and improve the SNR, such a circuit is an important addition.

What was known from a very early stage was that a differential amplifier was the prime candidate to handle this role. Initially, any differencing amplifier was thought to be capable of this undertaking. However, after consideration was afforded as to the ideal properties desired here, a distinction was made in the selection process. Within a subcategory of the differential amplifier family is the instrumentation amplifier. First suggested in frequently resorted to literature, this amplifier presents some significant characteristics in addition to those commonly seen in their standard differencing counterparts. These specific characteristics along with the factors which instigate their requirement will be briefly outlined now.

It is known that the strain gauge and the bridge in its entirety have relatively high impedance. This fact, coupled with the weak output signal, in the low millivolt range, incurs the potential for the amplifier to draw current from this circuit. Instrumentation amplifier are designed with a particularly high input impedance, typically in the range ( $10M\Omega$  to  $10G\Omega$ ), thus negating such a possibility.

Differential circuits, of which the Wheatstone bridge is one, have characteristically small output voltages, superimposed on a larger common-mode voltage. This common mode voltage is typically a significant measure of the excitation voltage and it is pertinent that it be rejected. An amplifiers measure of effectiveness for performing such a duty is the

common mode rejection ratio (CMRR)<sup>[9]</sup>. Instrumentation amplifiers offer a hefty CMRR relative to their more standard counterparts, typically boasting values in the range (100-140 dB).

These were the primary contributing factors for the preference of this particular amplifier. The more standard benefits of stability, precision gain and low offset voltage all apply in varying levels of significance dependent upon the specific model chosen.

Taking all of the aforementioned matters into consideration, the chosen instrumentation amplifier for this project was the Texas Instruments INA122P<sup>[10]</sup>. Without delving too deeply into the technical aspects of the chip, which can all be found in the referenced datasheet, the most important parameters are highlighted here in Table 2.

Table 1: Key Specifications of the Texas Instruments INA122P

Parameter	Value
Supply Volt. Range	2.2V – 36V
Input Impedance	$10^9 \Omega$
CMRR	94 dB (typ)
Offset Voltage	250 $\mu$ V (max)
Gain Range	5 – 10000
Bandwidth (G=100)	20 kHz

Table 2: INA122P Instrumentation Amplifier Parameters as per the Datasheet

Setting the gain, applicable to the range as outlined in Table 2, is done according to the gain equation as it appears in Equation 4. This range is entirely suitable for the requirements of the project and a gain anywhere in the region of G=80-200 would likely be within the workable limits. Details of the exact gain chosen will be elaborated on further in Section 2.1.

$$G = 5 + \frac{200k\Omega}{R_G} \quad (4)$$

As per the official datasheet this amplifier supports the use of both single and dual power supply configurations. While this may be the case for a number of circumstances, it was not found to be the case here. More on how this came to light and the subsequent ramifications can be found in Section 2.1 or within the Logbook which accompanied this experiment.

### CANTILEVER DEFLECTION

The physical phenomena at play throughout the mechanical deflection of a cantilever are of great importance in this project. The root of the entire height measurement process is founded on the properties at play here. Being able to reliably predict the response of this device to a given impulse ranks very highly on the list of key aspects for the accurate completion of such an undertaking.

Cantilevers come in multiple forms, though possibly obvious to the reader, its important to understand which one in particular is being utilized here. The fixed-free cantilever happens to be as simple as they come. The key parameters that influence the mechanical response to a given force are the length of the beam (L), the inertial moment (I), and the Young's modulus (E).

These parameters each play a key role in Equation 5 seen below. This equation outlines the relationship between deflection ( $\delta$ ) of the cantilever for a given force (F) impinged on the free extremity<sup>[11]</sup>.

$$\delta = \frac{FL^3}{3EI} \quad (5)$$

With that the applicable theoretical concepts, necessary for the uninhibited understanding of the details of this report, have now been outlined. Should additional reading with regard to any of these specific categories be desired, some such sources of information have been included under the Additional Reading subsection of Section 5.

## 2 METHODOLOGY

### 2.1 APPARATUS

The physical production of the cantilever device accompanied with its circuitry comprised a central role and lengthy role in the overall scheme of this project. Many avenues of approach were considered and in certain cases pursued for a period of time. Where an approach was ultimately ceased but determined to provide additional insight to the nature of the device, it has been included in this section. One such example, as alluded to earlier, was the initial design choice centred around the use of four strain gauges in a full configuration Wheatstone Bridge. This pursuit is noteworthy and as such will be detailed until the point at which the determination was made to alter the number of gauges.

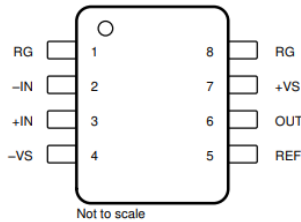


Figure 3: Pin Diagram for the INA122P Amplifier Chip

### Preliminary Approach

The foundational work, having collected the necessary components as outlined in Section 1.2, was to test each item individually. In doing so a greater appreciation for the manner in which they contribute to the project was gained. The suitability of a strain gauge and metallic ruler type cantilever was tested using similar models of both which were fortunately at the disposal of the team. The ruler was fixed at a given length and the resistive fluctuations of the strain gauge (pre-installed on the beam) were observed. This initial trial indicated approximately  $\pm 0.3\Omega$  variations for

reasonably strong strains. Such figures, in alignment with what was purported, afforded a level of confidence in the ability of this apparatus going forward.

Similar trials of the amplifier were conducted in order to establish the correct order and functionality of its pins, as seen in Figure 3.

### Construction

The construction of the apparatus began with the strain gauge and cantilever device. From Section 1.2, it is known that the greatest strain experience by a fixed-free cantilever is experienced at the fixed extremity and decreases linearly towards the free extremity. As prefaced here, four strain gauges were to be fixed to the cantilever. Given the fact that at any point 2-3 of these devices could be uninstalled from the circuitry, their inclusion was doubtless the appropriate choice. Once the positioning was determined, wherein two gauges sit opposite each other toward the fixed end and two in equivalent tandem toward the free end, they could then be mounted.

A cyanoacrylate adhesive, as specified in the Radionics datasheet<sup>[12]</sup>, was used for the purpose of fixing the strain gauges to the surface of the ruler. The surface was first cleaned before a reasonable amount of adhesive was applied. The strain gauges were then individually placed, in a careful manner, onto the adhesive locations and pressed down to ensure solid contact had been made. Given the delicate nature of the gauges, any lifting of the body off of the contacted surface could result in inaccuracies later in the process.

With the gauges fixed in place, the contact pads were then set down using their self-adhesive backing, at a suitable distance in proximity to the legs of each device. Before soldering took place, wires long enough

to reach the accompanying circuit were cut for this purpose. Each set of wires were then manipulated into twisted wire pairs. Though this approach of twisted wire pairs can certainly help to reduce noise in due to electromagnetic fields, the main purpose here was actually to maintain a neat wiring structure. Neatness of circuitry and wiring is paramount to the potential troubleshooting that is necessary later in projects akin to this one.

With the wires prepared, the exposed end of each were placed on the contact pads alongside the respective legs of the strain gauges, where soldering could then take place. After this process concluded, each pad was tested for successful connection and it was ensured that no cross-contact was present. The unused ends of the twisted wire pairs were then entered into a breadboard<sup>[13]</sup>, in the four resistor positions of a Wheatstone bridge circuit. In this circuit, two of the wire pairs connect from the positive supply to the main board and the remaining two connected respectively in series from the board to ground. The differential voltage can then be outputted from the nodes between the two sets of wire pairs. A similar representation of this is as seen in Figure 4. While this was the initial setup, the alteration made in order to convert this circuit to one suitable for a dual strain gauge setup, was to replace two of the four wire pairings with equivalent value resistors, i.e  $120\Omega$ .

The aforementioned outputs from the bridge then act as the inputs to the amplifier circuit. Where space allows, as was the case here, the amplifier circuit could neatly be arranged on the same breadboard as the Wheatstone bridge. Each output is wired into the -IN and +IN pin respectively, as they appeared in Figure 3. As outlined in Section 1.2, the possibility exists for this amplifier to be configured in a dual or single power supply setup. Initially, a single power supply setup was favoured for the simplifying nature of power arrangements

amongst the project group as a whole. However, made apparent through a series of tests, was the conclusive determination that the single power supply configuration as it appeared in the datasheet did not function accordingly.

With the fact now established that the single power supply would not work for out circuitry, the dual power supply configuration was deemed to suffice. Voltage supply of  $\pm 5V$  was setup on the rails of the breadboard and wired into the V+ and V- pins of the chip. While multiple gains were also tested, the most appropriate appeared to be G=100. Accounting for the bridge output being in the range  $\pm 5 - 10mV$ , a gain of this magnitude returns values typically in the 0 – 1V range when accounting for appreciable offset and other inherent variations. To set this gain Equation 4 was rearranged in order to calculate the required gain resistor  $R_G$ .

$$R_G = \frac{200k\Omega}{100 - 95} \approx 2105\Omega$$

This indicates that a  $2.1k\Omega$  resistor ought to be placed across the 1-8 pins of the INA122P. With that, the final step in configuring the amplifier circuit is to ground the unused reference pin  $V_{ref}$ . Unfortunately, this was unbeknownst to the author in preliminary research and caused a moderate deal of confusion. Where this pin is grounded no such offset should appear in the voltage output. Now that the amplifier is setup, the single ended output is suitable for measurements to be taken and the calibration process to begin.

## 2.2 CALIBRATION

The calibration of such a device is paramount to the accurate return of height measurement. As such, various methods of completing this process in the most accurate manner

were considered. While ideally, the deflection of the cantilever itself could be directly related to change in output voltage from the circuit, this proves a more difficult task where accurately determined incremental deflections are required. The use of a micrometer was touted as a possible manner in which this could be executed, however, given the difficulty securely mounting the micrometer and cantilever in suitable positions, alternate methods were sought.

The situation in which greatest controllability was predicted, was that of a hook and mass calibration, wherein a hook is attached to the free end of the cantilever and known masses are added successively. Before beginning this process, the cantilever must be fixed in place at the correct length. The easiest way to ensure reliability in the calibration was to first integrate the device into the proposed permanent position on the extruder box of the 3D printing rig. To hold the cantilever in place, alongside a number of other adjacent components, two portable vice clamps were utilized to impose a secure hold.

With the cantilever in place, the accompanying circuit was secured at a suitable distance on the exterior of the printing rig. The calibration process could now begin. The weights procured for this undertaking were a uniform set of calibrated laboratory weights. Each member of the set was weighed individually on the laboratory scales to ensure the accuracy of the apparent values and any discrepancy or error noted. All error and uncertainty have been detailed in Section 3.2 should further interest need satisfaction.

Initial readings of the cantilever were recorded prior to weight being added. Once it was observed that outputs were in fact appreciably stable, the process of added weights began. For each addition of weight to the free extremity, a set period of time was observed before the voltage was recorded. For the purpose of accurate voltage measurements the

standard digital multimeter (DMM) was not used here. In lieu of this, the AIM-TTi 1908 5½ digit benchtop multimeter was utilized. Once the maximum weight and this deflection was observed, the same process was then conducted in reverse. This final step of the calibration was added in order to check for hysteresis in the system. All results from this calibration can be found in Section 3.

## 2.3 SOFTWARE IMPLEMENTATION

Once the calibration equation has been successfully extracted following the completed calibration process, the output of the amplifier can then be routed to the National Instruments DAQ. Its implementation into an executable software program is then the next step in the process. While the end-goal on the software side of the project is naturally the synchronisation of each individual members code in an all encompassing script, creation of individual sub VI's and then subsequent amalgamation is the easiest route forward. The chosen software here is National Instruments LabView. For those unfamiliar, this is a graphically oriented coding environment which uses G, its native dataflow-based language.

Using LabView, the DAQ assist function was utilized to output the voltage value being read from the amplifier circuit output. This voltage was then treated with the calibration equation as found previously. As alluded to previously in Section 1.2, the voltage to mass equation does not equate to deflection. Instead, Equation 5 ought to be incorporated in order to get a true deflection value. As such, treating the force ( $F$ ) as  $(M \times g)$  the equation returns the following relationship, which calculates a value of deflection in metres.

$$\delta = \frac{(9.8ms^{-2})(0.13m)}{(3)(190 \times 10^9 Pa)(2.81 \times 10^{-12}m^4)}$$

$$= 0.013 \cdot M$$

The other crucial component of the standalone coding infrastructure before the amalgamation of code is concerned, is the implementation of a digital tare. Given the finicky nature of strain gauges and the circuitry that accompanies them here, it is only natural that the offset seen in the calculated calibration equation differs slightly from that seen at the beginning of any given session. As such, the voltage, where no appreciable deflection is imparted, ought to be counteracted in order to display a zero deflection measurement. The idea of a digital tare is to allow such a zeroing at any given moment.

In order to implement this mechanism, a boolean comparison logic was devised. Using a comparison block, triggered by a boolean constant, the current value of voltage outputted from the DAQ can be written to a local variable. At any other point in the coding structure, a ‘read’ equivalent for the same local variable can be subtracted from the DAQ assist output.

Though these are the building blocks behind the cantilever’s coding logic, the reader may understandably question as to where this fits into the overall, amalgamated coding structure. While detailed versions of the code may be referred to in the appendix, the following is the general running order of the code.

- 1** The Z-axis motor begins to lower, until the photodiode array detects the laser which has been deflected off of the cantilever.
- 2** Once this threshold voltage is reached (i.e. the tip of the cantilever has reached the object being scanned), the cantilever output is set to tare. Zero deflection should now be outputted.
- 3** Simultaneously, the raster scanning motion in the X-Y plane and the continuous

recording of objects height occurs. The height values are then compiled into an array before being written to a .csv file.

- 4** Utilizing specified X-Y arrays along with the newly created Z-height array, the data is now ready for post processing.

## 2.4 TESTING PROCEDURE

With the completion of the software implementation and the full integration of both the components outlined here as well as the laser and photodiode array, the testing of the entire system can commence. This process within the overall scheme of such a project can become rather convoluted. In order to ease the difficulty that can arrive with the amalgamation of a number of individual components it must be assured that a robust procedure is adhered to.

This procedure involved the testing of each component in order of utilization to ensure that the integration process had been completed without provoking any further issues. Testing each stepper motor on a separate coding script, the laser and photodiode, and finally the cantilever device all took place before commencement of the overall tests.

Once these formalities had concluded the master copy of the LabView code was initialized as specified in the previous section. With the system ensured to share a common ground, the power supplies were switched to output and the device allowed to operate in the absence of any sample test piece. The lack of a test piece here was purely to ensure that a synchronous harmony played out between the respective components.

Further testing was layered incrementally in complexity, with the additional tests of laser voltage thresholds, cantilever tareing techniques, differing test pieces, scan sizes and more.

### 3 RESULTS & ANALYSIS

#### 3.1 DEFLECTION MEASUREMENT

The results of the outputted deflection measurements varied periodically over the course of the project as different approaches and methods were tested and implemented. The following results represent those obtained in the finalized configuration as has been outlined previously throughout Section 2. All error and uncertainty values included within this section are a result of the workings which can be referred to in Section 3.2.

#### Calibration

The most stable calibration procedure successfully undertaken proved to be that which was described previously, wherein calibrated masses were added sequentially to the free extremity of the cantilever. The range of masses and the recorded voltage values from the output of the amplifier circuit can be seen below in Table 3. The corresponding plotting of these values is shown in Figure 4, though the masses have been multiplied by the ac-

celeration due to gravity in order to plot the more desirable Force versus Voltage relationship.

Readily apparent from this calibration plot, is the precisely linear relationship between the applied Force and the output voltage. This aligns with predictions and can therefore be fitted using a rudimentary linear fitting as seen in red on the graphic. Though small, error bars have been included this plot, as calculated in Section 3.2.

Using the linear fitting function that has now been created, the equation of this line corresponds to that of the calibration equation. This equation was returned as:

$$V = (0.1036 \pm 0.001)F + (2.7818 \pm 0.006) \quad (6)$$

Should it be of interest to the reader, additional calibration data for the unused quarter-bridge and full-bridge configurations of the Wheatstone bridge have been included in the Appendix.

Mass (g)	Voltage (V)
0	2.788
100	2.887
200	2.996
300	3.075
400	3.178
500	3.279
600	3.390
700	3.494
800	3.610

Table 3: Mass added to cantilever vs. amplified bridge output voltage.

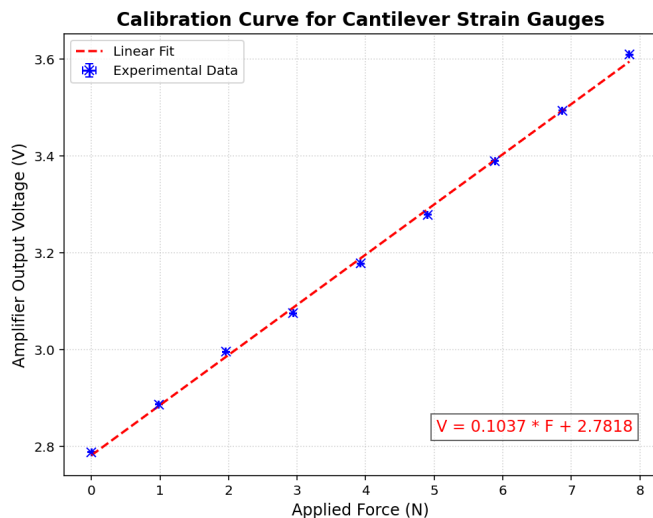


Figure 4: Calibration curve, corresponding to data seen in Table 3 - showing relationship between output voltage versus Force

## Output Testing

Given the completion of a seemingly satisfactory calibration and the production of the Equation 6, the calibration equation, preliminary testing of the deflection outputs was decided upon. These tests served as rudimentary guidelines for the accuracy of the cantilever readings, primarily intended to indicate whether overall integrated system tests could commence. As such the data sets were brief in depth and rigour. Nevertheless their inclusion here ought to justify the accuracy of the calibration equation seen previously. The ‘true’ height increments in question, were that of a simple 3D printed set of stairs with step heights of 0.3cm up to a total Z height

of 1.5cm. The distinction between the results in ‘Deflection 1’ versus those in ‘Deflection 2’ is that the former utilized the standard Equation 6 calibration value. In contrast, the latter of the two headings utilized a value of double the stated calibration equation. This result is damning of the calibration equation in the sense that its closest percentage difference was that of 65.47% in comparison with the doubled values optimum percentage difference value of 9.67%. Though an unfortunate finding, it highlights the misbehaviour of the original calibration and had time allowed within the boundaries of this report’s submission, would have allowed for a fresh attempt with a result in the region of  $V = (0.20 - 0.30)F$  expected.

Increment (cm)	Voltage(V)	Post Tare	Deflection 1(cm)	Deflection 2 (cm)
0.0	2.746	0	0.000	0.000
0.3	2.614	-0.132	0.545	0.271
0.6	2.496	-0.250	1.032	0.513
0.9	2.360	-0.386	1.594	0.793
1.2	2.254	-0.492	2.032	1.010
1.5	2.145	-0.601	2.482	1.235

Table 4: Experimental data with percentage differences.

## 3.2 ERROR ANALYSIS

[14] Throughout an experimental process such as the one described here, many sources of error and uncertainty arise. While simple to catalogue initially, it is vital that the propagation of these metrics be carefully monitored and treated appropriately. The primary sources of error here come in the form of instrument resolution and uncertainty, opera-

tor fault, inherent equipment error, and assumptions of certain unknown values such as Young’s modulus.

These uncertainties present themselves primarily in the calibration process, deflection equation, and general signal acquisition. Each individual measurement value is first addressed in a compartmentalized manner. Where uncertainties combine, a propagation treatment is required, as detailed below.

## CALIBRATION

### MASS UNCERTAINTY

Given a mass measurement uncertainty of  $\pm 0.5 g$ , the force uncertainty is:

$$\Delta F = \Delta m \cdot g$$

### DMM UNCERTAINTY

For the DMM used here the following specification apply:

$$\text{Accuracy} = 0.02\%, \quad \text{Resolution} = 1\mu V$$

Total voltage uncertainty:

$$\Delta V = 0.02V + \text{Resolution}$$

$$\Delta V = 0.02V + 1 \times 10^{-6}V$$

### REVISED CALIBRATION EQUATION

Applying the above uncertainties to the Python plotting script for the calibration values, the following revision of the calibration equation is computed:

$$V = (0.1036 \pm 0.001)F + (2.7818 \pm 0.006)$$

## DEFLECTION EQUATION

The deflection of a cantilever beam under a force  $F$  at length  $L$  is as previously stated in Equation 5:

$$\delta = \frac{FL^3}{3EI}$$

Uncertainties in the parameters contribute to the total uncertainty. Given the length of the following equations, a wide format will temporarily be utilized:

$$\frac{\Delta\delta}{\delta} = \sqrt{\left(\frac{\Delta F}{F}\right)^2 + 9\left(\frac{\Delta L}{L}\right)^2 + \left(\frac{\Delta E}{E}\right)^2 + \left(\frac{\Delta I}{I}\right)^2} \quad (7)$$

With given values:

$$\Delta F = 4.9 \times 10^{-3}N, \quad \Delta L = 1 \times 10^{-3}m, \quad \Delta E = 2\% \times 190 \text{ GPa}$$

### INERTIAL MOMENT

Before continuing Equation 6, we must first examine the final term, which represents the relative uncertainty in the moment of inertia. As known from Section 1.2, this requires further propagation. Using the equation for the moment of inertia and the recorded values

with associated uncertainties:

$$I = \frac{bh^3}{12}.$$

$$\Delta h = 1.05 \text{ mm} \pm 1 \times 10^{-2} \text{ mm}, \quad \Delta b = 29.13 \text{ mm} \pm 1 \times 10^{-2} \text{ mm}$$

$$\frac{\Delta I}{I} = \sqrt{\left(\frac{0.02 \text{ mm}}{29.13 \text{ mm}}\right)^2 + 9\left(\frac{0.03 \text{ mm}}{1.05 \text{ mm}}\right)^2}$$

$$\boxed{\frac{\Delta I}{I} = 9.579 \times 10^{-4}}$$

### AVERAGING VALUES APPROACH

Since force varies continuously, an averaging approach is employed to reduce large relative errors for small force values. The mean of the force values is calculated as:

$$F_{\text{avg}} = \frac{1}{N} \sum_{i=1}^N F_i \quad (8)$$

Deflection is then calculated using the  $F_{\text{avg}}$  value, obtained from the dataset and given as  $F_{\text{avg}} = 3.92N$ :

$$\delta_{\text{avg}} = \frac{F_{\text{avg}} L^3}{3EI}$$

$$= \frac{(3.92N)(0.13m^3)}{3(190 \times 10^9)(2.81 \times 10^{-12})}$$

$$\delta_{\text{avg}} = 5.38 \text{ mm}$$

### FINAL DEFLECTION UNCERTAINTY

$$\frac{\Delta \delta}{\delta} = \sqrt{\left(\frac{4.9 \times 10^{-3}N}{3.92N}\right)^2 + 9\left(\frac{1 \times 10^{-3}m}{0.130m}\right)^2 + \left(\frac{2\% \times 190 \text{ GPa}}{190 \text{ GPa}}\right)^2 + (9.579 \times 10^{-4})^2}$$

$$\boxed{\frac{\Delta \delta}{\delta} = 0.088 = 8.8\%}$$

### 3.3 TOPOGRAPHICAL OUTPUT

Though in hindsight, the trustworthiness of the calibration equation used here is doubtful, as witnessed in Section 3.1, it was utilized in the testing of the overall system. This was done in the interest of progression under the limiting time constraints of the project and

in order to establish the working order of the device as a whole. Given the overarching goal of the project is to produce a topographical image of a given surface, even one indicate of the true contours lends itself to the idea that such a device is capable of being produced in the manner outlined.

Rough Reconstruction of the intended Sample Surface

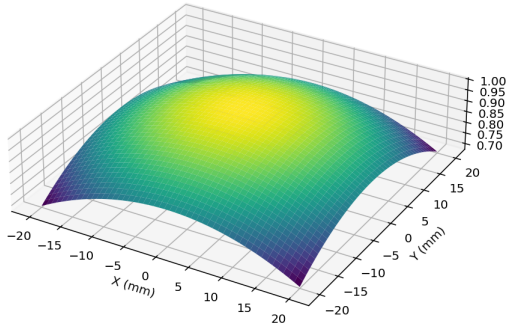


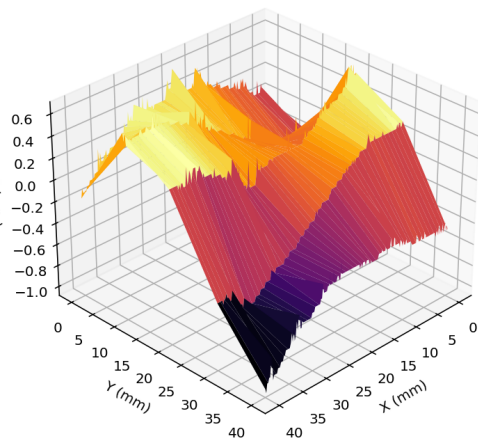
Figure 5: The graphical reconstruction of the test piece used for comparison with produced plots seen in Figure 6.

As of the time of writing, a single test of the apparatus was completed in its entirety. This test confirmed that the constituent components were successfully installed and code scripts amalgamated harmoniously. The test piece in question here bore the shape of a flattened dome, ideal for the non-impeding testing sought, while also providing constant height deviation. A rudimentary reconstruction of the object can be seen in Figure 5.

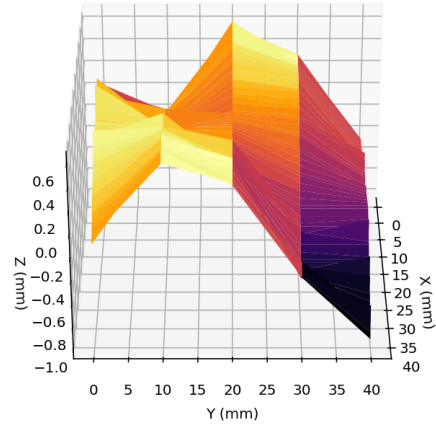
Below in Figure 6 (a-c), the surface profile as

produced by the system testing can be observed from multiple differing perspectives. Readily apparent is the ungainliness of the reproduction, though the relative displacement suggests that with greater testing and troubleshooting, far greater accuracy may yet be achieved with this device.

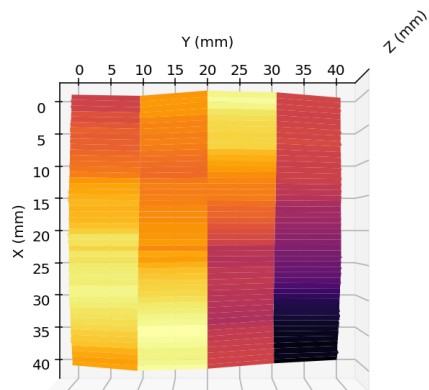
Multiple factors may have induced such noise and variability, these will be discussed in some detail in Section 4.



(a)  $45^\circ$  X-Y View



(b) Elevated Y-Plane View



(c) Top Down View

Figure 6: Different Perspective Views of the System

## **4 DISCUSSION & CONCLUSION**

### **4.1 SUMMARY OF FINDINGS**

With the culmination of this eight week collaborative effort into the design, development, and subsequent investigation of a surface profilometer, vast learnings have been accumulated.

Throughout the preliminary theoretical investigation, the nature of each component was stripped back and a greater understanding of components such as instrumentation amplifiers, strain gauges, Wheatstone bridges and more was developed. The technical aspects necessary for the successful interfacing of specific components was ensured and strong foundations for the undertaking of this project were set.

Though much deliberation ensued over various configurations of components, such as the selections of the number of strain gauges used or the power supply of the amplifier circuit, the crux of each conundrum was routed out and justifications of every step outlined in full. The choice, ultimately, to employ a half-bridge Wheatstone bridge configuration, with both strain gauges facing opposite each other on the cantilever, proved the most effective method. With the benefit of stability on its side over the full four gauge setup, yet maintaining a greater resolution than the single gauge, the compromise was deemed worthy.

The physical integration of constituent components, though tricky given the working dimensions of the printer housing, progressed smoothly and resulted in the harmonious synchronization of all moving parts and otherwise. The LabView code which empowers the entire system is comprised of an seamless of the codes created by individual team members. While dense in appearance, through much troubleshooting, the final product performed its task with distinction according to

all available testing.

The calibration of the cantilever, while satisfactorily undertaken, provided a result which, after testing, appears to be a factor of two too large. This misgiving resulted in some smaller numbers in the limited testing afforded to the team. Nevertheless, the linear action of the device in response to increasing and or decreasing step values signifies that, with a little more tinkering, the cantilever ought to be suitable for the task at hand. Final testing of the system, in its final form, resulted in slightly noisy, and somewhat skewed reproduction of the intended test piece. With that said, the overall spirit of the test piece remained intact. That is to say that though the particular smoothness of the piece was lost, the contours and general form of the surface were captured in a relatively accurate manner. This result implies a great deal of hope be afforded to the future development of the surface profilometer and with more time invested in the testing of the device, a great level of accuracy may be achievable.

### **4.2 FUTURE IMPROVEMENTS & APPLICATION**

While the current iteration of this device may be of little application at this stage of its development, there is certainly great scope for the betterment of its functionality in the near future.

While working with the device itself, it is readily apparent that its use, should resolution be enhanced, may come in a maelstrom of forms. One such use may be its application in the digitization of any particular item one desires. For example, instead of creating a laborious digital model of an object, the surface profilometer could be a quick and seam-

less way to recreate it. If it could be interfaced with a CAD like program or perhaps a graphics design software, the possibilities in this field are undoubtedly plentiful.

Specific improvements to the device have been proposed in many forms throughout the project, with multiple appearing in the accompanying project logbook. In a future iteration, the idea of utilizing the laser and photodiode array as an additional form of height measurement would be highly desir-

able. The dual approach to deflection measurement could be melded into a single system wherein the statistical average of their values be utilized for the final output.

As for the cantilever device in particular, the installation of an automatic calibration program has been tentatively looked into since the calibration process began. Though this implementation has not investigated as of the time of writing, its proposed benefit is merit enough in itself for great consideration.

## 5 BIBLIOGRAPHY

### REFERENCED MATERIAL

- [1] Horowitz, P. & Hill, W. (2015) *The Art of Electronics*. 3rd edn. Cambridge: Cambridge University Press, p. 297.
- [2] RS Components (2022) *RS PRO Low Profile Strain Gauge Datasheet*. RS Components. Available at: <https://docs.rs-online.com/6e83/A70000008880717.pdf> (Accessed: DATE).
- [3] National Instruments (2016) *Strain Gauge Measurement – A Tutorial*. National Instruments. Available at: [https://elektron.pol.lublin.pl/elekp/ap\\_notes/ni\\_an078\\_strain\\_gauge\\_meas.pdf](https://elektron.pol.lublin.pl/elekp/ap_notes/ni_an078_strain_gauge_meas.pdf) (Accessed: DATE).
- [4] Omega Engineering (2021) *Practical Strain Gage Measurements*. Omega Engineering. Available at: [https://www.omega.co.uk/techref/pdf/straining\\_gage\\_measurement.pdf](https://www.omega.co.uk/techref/pdf/straining_gage_measurement.pdf) (Accessed: DATE).
- [5] Roe, M. (2025) *IDT Project Proposal*. Atlantic Technological University.
- [6] Halliday, D., Resnick, R. & Walker, J. (2013) *Fundamentals of Physics*. 10th edn. Wiley.
- [7] All About Circuits (2019) ‘Strain Gauges — Electrical Instrumentation Signals’, *All About Circuits*. Available at: <https://www.allaboutcircuits.com/textbook/direct-current/chpt-9/strain-gauges/> (Accessed: DATE).
- [8] Fraden, J. (2016) *Handbook of Modern Sensors: Physics, Designs, and Applications*. 5th edn. Springer.
- [9] Texas Instruments (2024) *INA122P Precision Instrumentation Amplifier Datasheet*. Texas Instruments. Available at: <https://www.ti.com/lit/ds/symlink/ina122.pdf?ts=1741699897101> (Accessed: DATE).
- [10] Roe, M. (2025) *IDT Project Logbook*. Atlantic Technological University.
- [11] Gere, J. M. & Timoshenko, S. P. (1997) *Mechanics of Materials*. 4th edn. PWS Publishing.
- [12] Hibbeler, R. C. (2014) *Mechanics of Materials*. 9th edn. Prentice Hall.
- [13] AIM-TTi (2024) *5 1/2 Digit Digital Multimeter Datasheet*. AIM-TTi. Available at: <https://www.farnell.com/datasheets/3674414.pdf> (Accessed: DATE).
- [14] Lira, I. (2002) *Evaluating the Measurement Uncertainty: Fundamentals and Practical Guidance*. Institute of Physics Publishing, ch. 5.

## 6 PLAGIARISM DECLARATION

<b>Student Name / Number</b>	Mark Roe - G00440145
<b>Programme</b>	Physics & Instrumentation
<b>Year</b>	Year 3
<b>Module</b>	Instrument Design Team Project
<b>Lecturer</b>	Dr. Oran Morris, Dr. Jennifer Quirke, Dr. Brian Ashall
<b>Assignment Title</b>	Surface Profilometer
<b>Date Submitted</b>	March 12th, 2025

I understand that plagiarism is a serious academic offence, and that ATU deals with it according to the ATU Policy on Plagiarism.

I have read and understand the ATU Policy on Plagiarism and I agree to the requirements set out therein in relation to plagiarism and referencing. I confirm that I have referenced, paraphrased, and acknowledged properly all sources used in the preparation of this assignment. I understand that if I plagiarise, or if I assist others in doing so, that I will be subject to the procedures outlined in the ATU Policy on Plagiarism.

I understand and agree that plagiarism detection software may be used on my assignment.

I declare that, except where appropriately referenced, this assignment is entirely my own work based on my personal study and/or research. I further declare that I have not engaged the services of another to either assist in or complete this assignment. Where such services are legally allowed and encouraged, I have acknowledged the same in this assignment.

Signed: \_\_\_\_\_

Date: \_\_\_\_\_

## 7 APPENDIX

### Additional Circuit Sketches / Diagrams

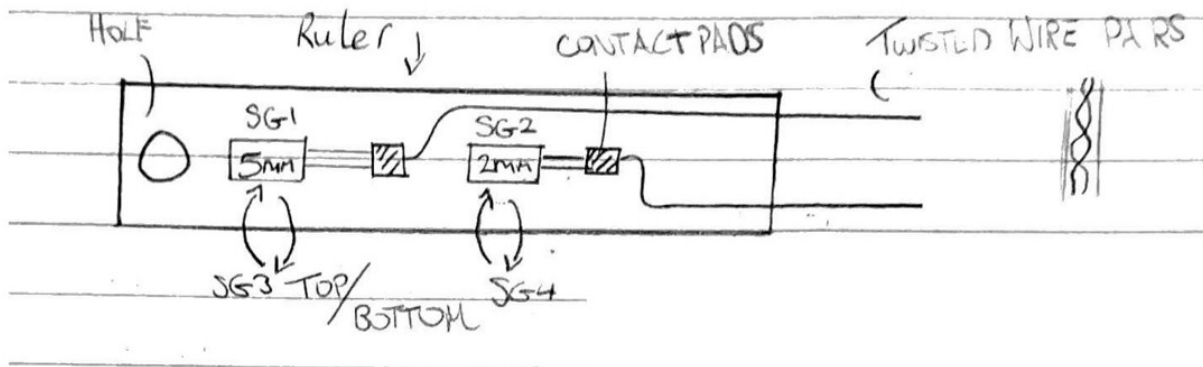


Figure 7: Original cantilever schematic

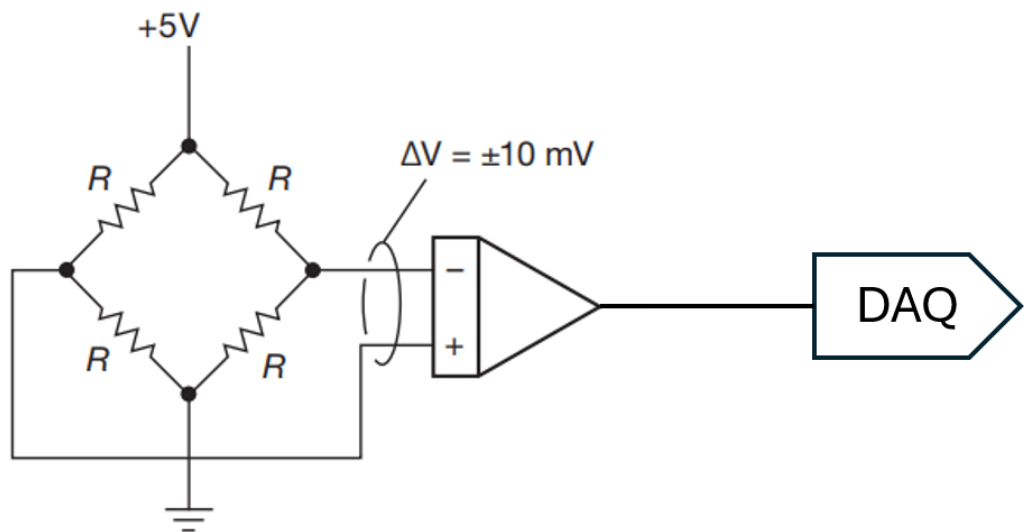


Figure 8: Basic wheatstone bridge to instrumentation amplifier and DAQ circuit schematic

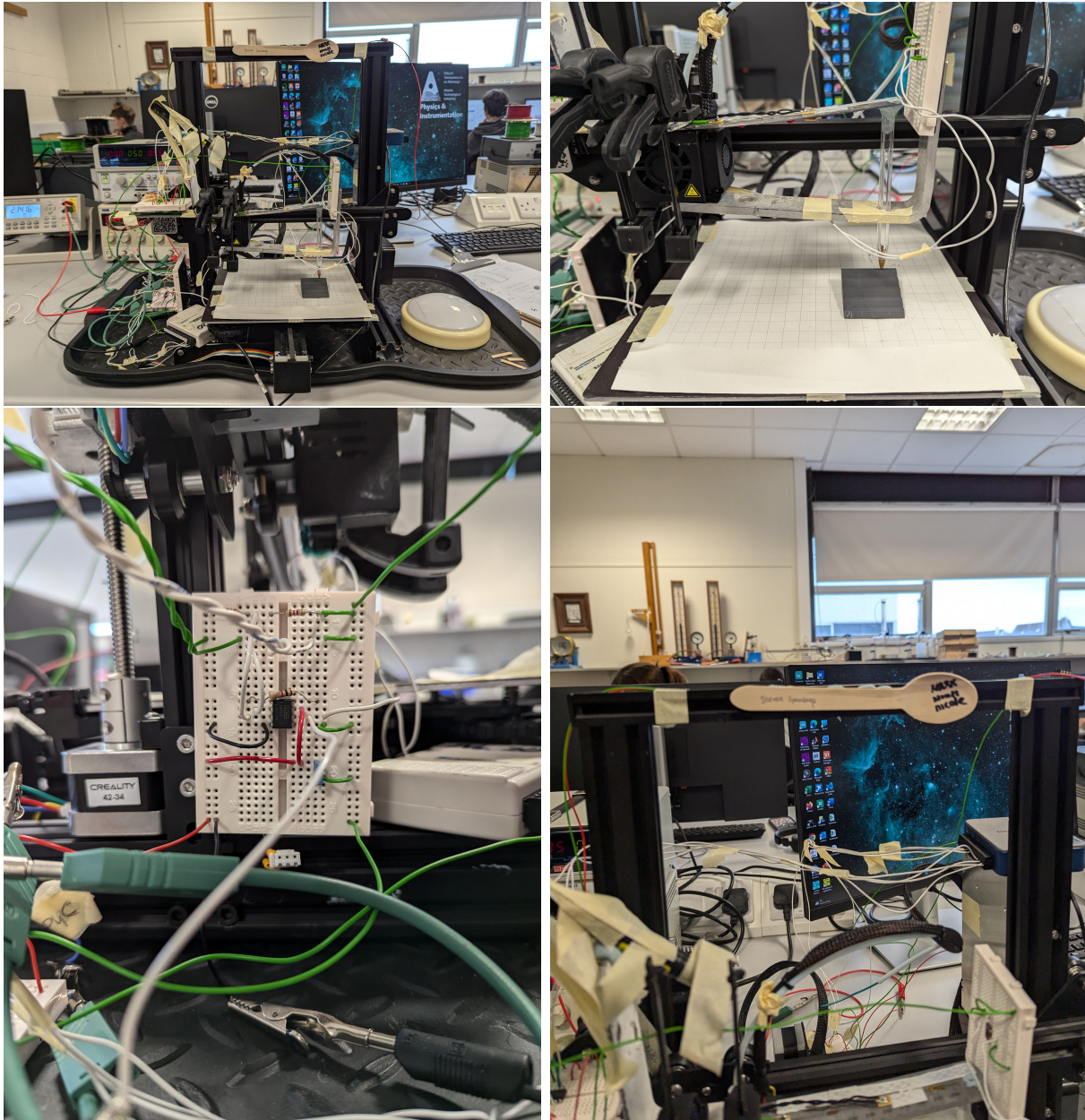


Figure 9: Images of the finalized Surface Profilometer displayed in the laboratory

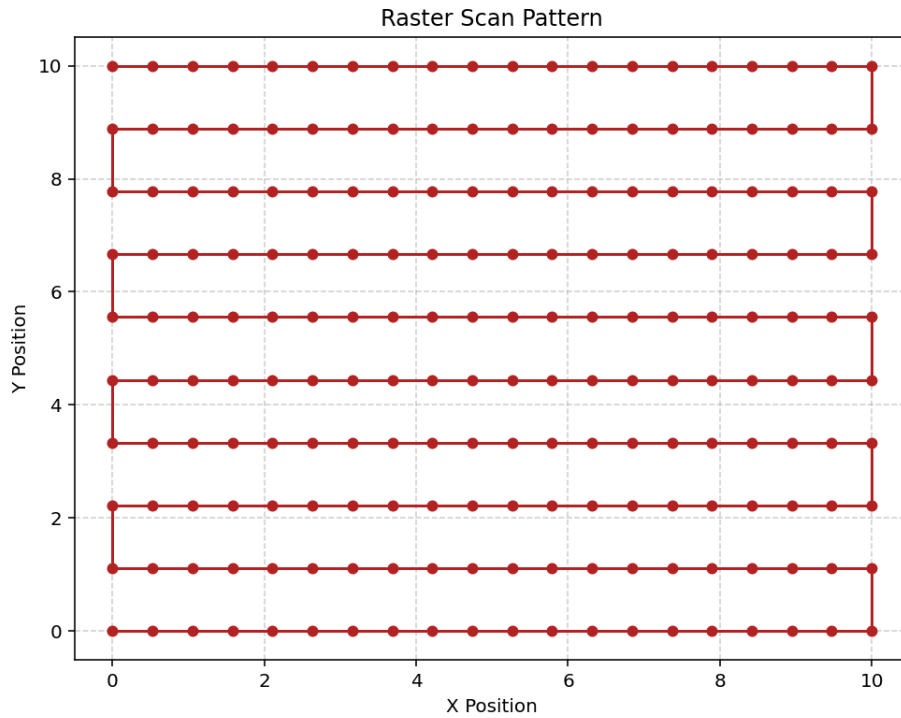


Figure 10: Indication of the raster scanning XY movement pattern

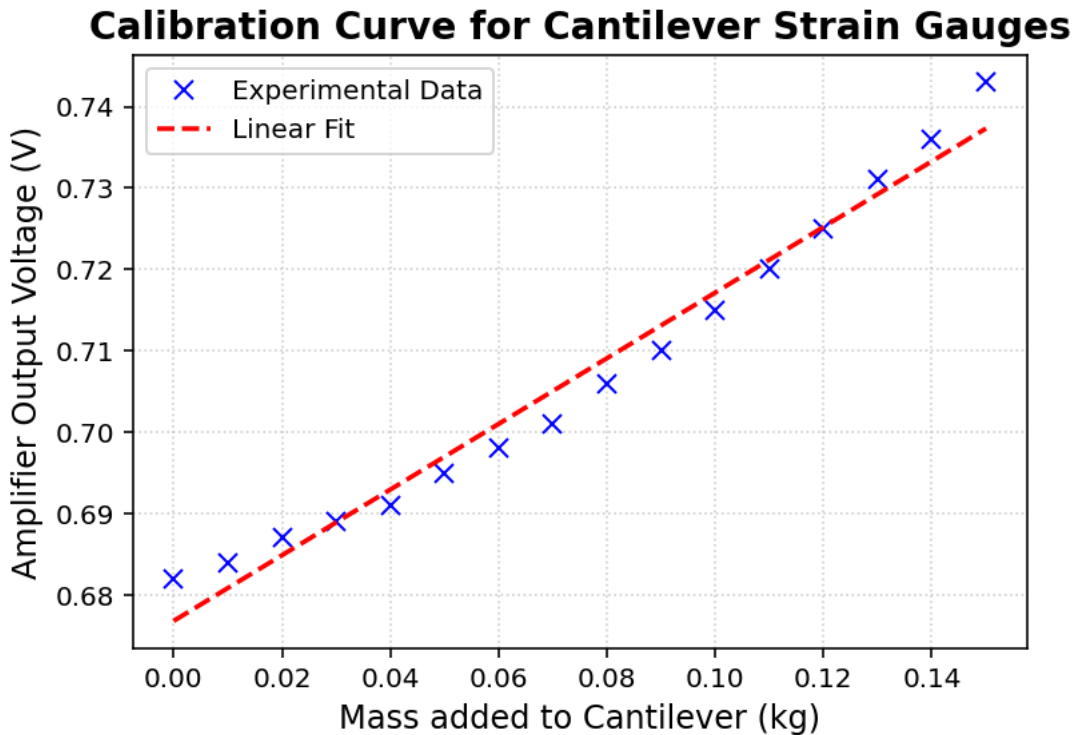


Figure 11: Original Calibration curve for the four strain gauge setup

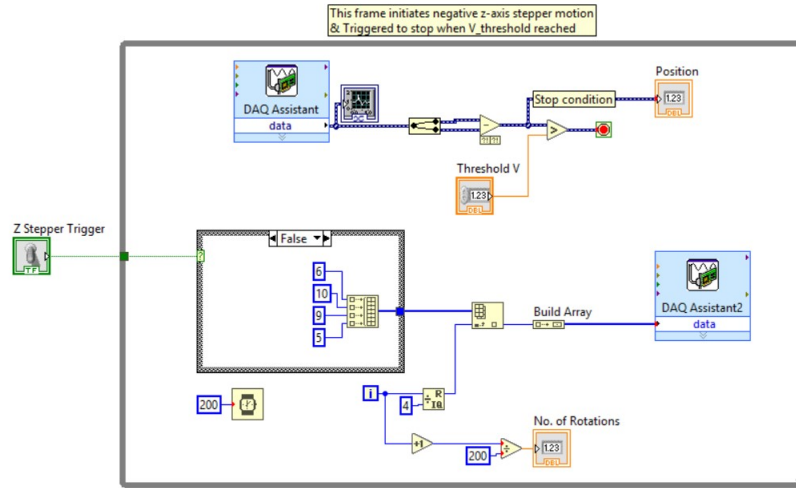


Figure 12: Z-motor code sample

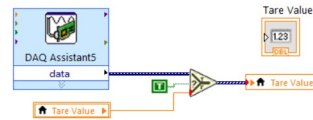


Figure 13: Cantilever digital tare of output code sample

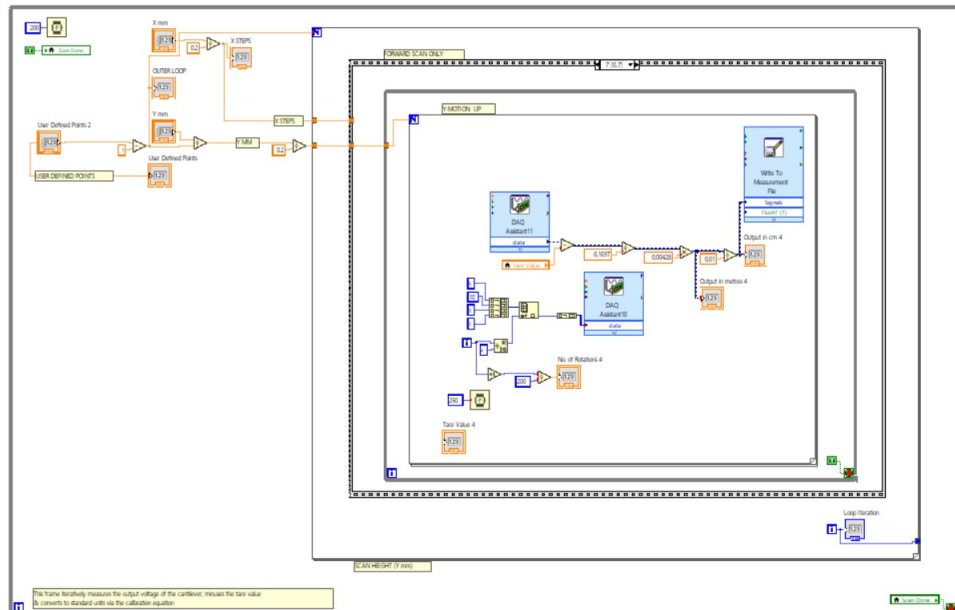


Figure 14: X-Y stepper motor and height value extraction code sample